Characterization of Colloid Thruster Beams

IEPC-2005-302

Presented at the 29th International Electric Propulsion Conference, Princeton University, October 31 – November 4, 2005

M. Gamero-Castaño and J. Ziemer
Jet Propulsion Laboratory, California Institute of Technology, Pasadena, CA , 91108, USA

Abstract: Colloid thrusters are electrostatic accelerators of charged droplets and ions generated by electrosprays. The low thrust and high thrust stability associated with a single emitter are ideal for precision spacecraft positioning applications. This technology will be tested in the Disturbance Reduction System-Space Technology 7 mission, which is a precursor of the Laser Interferometer Space Antenna mission. Although the colloid thruster engine for DRS/ST7 is at an advance stage of development, and key performance parameters (e.g. thrust level, throatability and noise; thruster lifetime) have been demonstrated, the structure of the electrospray beam is largely unknown. A good knowledge of the beam is necessary to assess its interaction with spacecraft surfaces, and to design optimally the accelerating electrodes of the thruster. In this article we use retarding potential, time of flight, and a Faraday cup, to measure the energy and specific charge distributions of the electrospray particles as a function of the position within the beam, as well as beam profiles. This information is then used, together with a model of the beam, to calculate its spreading.

I. Introduction

DETECTION of gravitational waves in space via projects such as LISA, as well as a variety of projected future missions involving formation flying of multiple spacecraft, require exquisitely fine thruster control, as well as the capability to use higher thrust levels for other maneuvers. Colloid thrusters may be the only technology that can provide both requirements simultaneously. Colloid thrusters will be demonstrated on NASA's ST7. Nevertheless, this technology is still in its infancy, and different thruster related phenomena are poorly understood and/or remain to be investigated. The spreading of the colloid thruster beam is one of such phenomena.

Knowledge on how the electrospray beam behaves, and the ability to manipulate it, can be used to improve two performance parameters of the colloid thruster: first, spacecraft contamination could be eliminated by reducing beam spreading; second, a larger beam current, and hence thrust, can be passed through the extracting electrodes if the beam spreading is reduced. The latter could increase considerably the throttling range of the colloid thruster, which would now have the potential to be used for cancellation of initial spacecraft tip-offs and safe mode actions, in addition to its nominal station keeping function.

The spreading of the beam is determined by two processes: initially, electrostatic forces induced by the beam's space charge opens up the beam. This happens along a microscopic region downstream of the emitter. Further from the emitter, the electric field of the space charge becomes negligible compared to the external field induced by the electrodes; in this macroscopic needle/extractor region, the spreading of the beam is modified by the force of the external electric field. This observation suggests a way to decrease beam spreading: optimization of the geometry and E-field of the extractor/emitter electrodes to focus the beam.

This article aims at developing a model of the spreading of colloid thruster beams, and is organized as follows: after this introduction, a simplified model of the beam spreading is given in section II.A. The experimental section II.B describes the main characteristics of a particular electrospray beam. Section II.C combines the simplified model and the experimental characterization to predict the spreading of the beam. Finally, the main results of our research and related future work are outlined in the conclusion section.

II. Discussion

A. Beam model

The expansion of a beam of charged particles in the emitter/extractor region is governed by the equation of motion of the particles (forced by the electric field), and the Poisson equation for the electric potential (induced by the electrodes and the beam space charge). They have to be solved together with the initial conditions for the particle trajectories (including positions and velocities, and a combined charge and mass distribution function for the particles), and the boundary condition for the electric potential (in the region where the particles are generated this boundary condition is time-dependent due to the dynamics of the jet breakup). In view of these complexities, we will use a simplified model to generate an approximate solution that exhibits the salient features of the beam spreading process. Taking advantage of the cylindrical symmetry of the problem, we divide the beam into *m* groups carrying currents I_i. The droplets within a group have the same specific charge, $<\frac{q}{m}>_i$. For higher accuracy, each group is further divided into *n* equal beamlets. The envelope of each beamlet, $R_{ij}(z)$, will be calculated using the equation of motion of a particle traveling along the beamlet envelope. The equations and initial conditions of the model are:

$$I_B = \sum_{i=1}^{m}\sum_{j=1}^{n} I_{ij} \qquad [1]$$

$$v_{ij}^2 \frac{d^2 R_{ij}}{dz^2} + v_{ij}\frac{dv_{ij}}{dz}\frac{dR_{ij}}{dz} = <\frac{q}{m}>_i \left[E_r^{spch}(R_{ij}) + E_r^{ext}(R_{ij})\right] \qquad [2]$$

$$v_{ij}\frac{dv_{ij}}{dz} = <\frac{q}{m}>_i E_z^{ext}(R_{ij}) \qquad [3]$$

$$\mathbf{E}^{ext} = -\nabla\phi^{ext} \qquad [4]$$

$$E_r^{spch}(R_{ij}) = \sum_{k=1}^{m}\sum_{l=1}^{n} F_{ij}^{kl}\frac{I_{kl}}{2\pi\varepsilon_0 v_{kl}} \quad \therefore \quad F_{ij}^{kl} = \begin{cases} 0, & R_{ij} < R_{kl} \\ \dfrac{1}{R_{ij}}, & R_{ij} \geq R_{kl} \end{cases} \qquad [5]$$

$$R_{ij}(0) = R_{jet} \quad [6], \qquad v_{ij}(0) = v_{jet} \quad [7], \qquad \left.\frac{dR_{ij}}{dz}\right|_{z=0} = 0 \qquad [8]$$

Equation [1] is the decomposition of the spray into *m*x*n* beamlets. [2] and [3] are the equations of motion (in terms of r(z) and axial velocity, $v_{ij}(z)$, rather than r(t) and z(t), of a particle traveling along the envelope R_{ij}. The electric field is divided in two terms: an external component induced by the electrodes, [4], and a component induced by the beam space charge, [5]; the latter is assumed to have only a radial component given by Gauss theorem. All the particles are assumed to be generated at a radial position equal to the radius of the jet, [6], with a constant axial velocity $v_{ij}(0)$ equal to the jet velocity, [7], and zero radial velocity, [8]. Other simplifications of the model are the use of: a constant specific charge for all the particles within a group $<\frac{q}{m}>_i$; the same axial velocity $v_{ij}(z)$ for the particles of a given beamlet; and the potential of the jet breakup point as the potential of the emitter.

The set of 2x*m*x*n* equations ([2] and [3]) are nonlinear and coupled. Furthermore, the external electric field does not in general have an analytical form. Therefore, the solution must be computed numerically. Despite this, it can be proved that for very small *z*, i.e. in the proximity of the emitter tip, the radial force induced by the space charge is

much larger than radial force caused by the external field, and we can use a simplified version of [2]. In addition, if prolate spheroidal coordinates are used to obtain an approximate expression for the external field, one can obtain the following approximate solution for the beam envelope, valid for small z:

$$R(z) \cong \sqrt{< \frac{q}{m} > \frac{1}{\pi \varepsilon_0 v_{jet}^3} \sqrt{I_B}} \sqrt{\mathrm{Ln}\left(\sqrt{< \frac{q}{m} > \frac{1}{2\pi \varepsilon_0 v_{jet}^3} \sqrt{I_B}} \frac{z}{R_{jet}} + 1 \right)}\, z \qquad [9]$$

$$v(z) \cong v_{jet}\left(1 + < \frac{q}{m} > \frac{\phi(0)}{v_{jet}^2 \mathrm{Arctanh}(\eta_{emitter})} \frac{z}{L(1-(D/L)^2)} \right) \qquad [10]$$

In Eq. [10], $\eta_{emitter}$ is the constant η–surface (a hyperboloid) representing the emitter in prolate spheroidal coordinates.[1] L is the distance between the focus of the hyperbola and the extractor plane, and D is the distance between the emitter tip and the extractor plane. With this result, we can estimate the axial distance $\tilde{z}$ at which space charge forces at the beam envelope become of the order of the second term in the LHS of Eq. [2]:

$$\tilde{z} \sqrt{\mathrm{Ln}\left(\sqrt{< \frac{q}{m} > \frac{I_B}{2\pi \varepsilon_0 v_{jet}^3}} \frac{\tilde{z}}{R_{jet}} \right)} = \frac{m}{q} \frac{v_{jet}^2 \mathrm{Arctanh}(\eta_{emitter})}{2\phi(0)} L(1-(D/L)^2) \qquad [11]$$

Shortly downstream, space charge forces become negligible and fall out of the problem as long as $\frac{dR}{dz} \geq 0$.

B. Beam characterization

Obtaining good agreement between experimental and model results depends critically on a precise estimate of the initial conditions for the particle trajectories (or equivalently in our model, the jet velocity and its radius), the boundary condition for the emitter potential (i.e. the potential of the jet at the breakup point), and the specific charge of the beam particles. Since there is no available analytical model for the breakup of charged jets that can provide accurate inputs, we will estimate these inputs by analyzing retarding potential and time of flight measurements of the beam droplets.

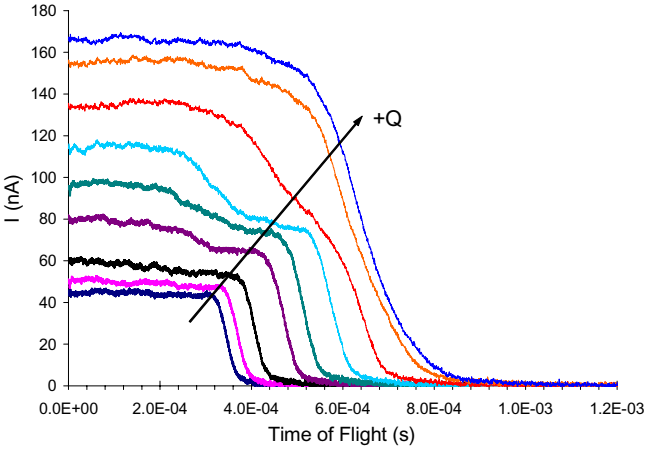

Figure 1. Time of flight spectra of PC/EMI-Im electrospray beams.

Figure 1 shows time of flight spectra of electrosprays of a solution of propylene carbonate mixed with 1-ethyl-3-methylimidazolium bis(trifluoromethylsulfonyl)imide (PC/EMI-Im). The spectra are for different flow rates, or equivalently for different beam currents (there is a one to one correspondence between both parameters). These beams feature bimodal droplet distribution (satellite and main droplets) for currents bellow approximately 140 nA. Satellite droplets appear when the Reynolds number associated with the jet capillary breakup exceeds a minimum value. Satellite droplets are smaller than main droplets and have larger specific charge, as can be inferred from the larger velocities in the time of flight spectra.

Figure 2 collects retarding potential curves for an $I_B = 87$ nA. The beam is sampled at different polar angles, i.e. the ArcTan of the ratio between radial distance from the beam axis (given in the figure legend), and axial distance from the emitter (20 cm). The bimodal distribution observed in the time of flight curves also appears in the retarding

potential spectra: the retarding potential of main droplets is centered around 1800 V (the emitter potential is 1820 V), while satellite droplets have much lower retarding potential, typically below 1200 V. Figure 3 shows time of flight spectra for the same beam current and for different polar angles. Note that figures 2 and 3 show a spatial separation of main and satellite droplets, the former being in the interior of the beam, while the latter appear in its outer region. This observation is more evident in figure 4, where we plot the charge flux of the beam as a function of polar angle for several beam currents, including $I_B = 87$ nA.

The above data can be used to estimate the velocity of the droplets at the point where they are formed, as well as the electric potential at this location.[2] First, we write the equation for the retarding potential of a droplet "i":

$$\phi_i^{RP} = \frac{1}{2}\frac{m_i}{q_i} v_i^2(\mathbf{x}) + \phi(\mathbf{x}) \qquad [12]$$

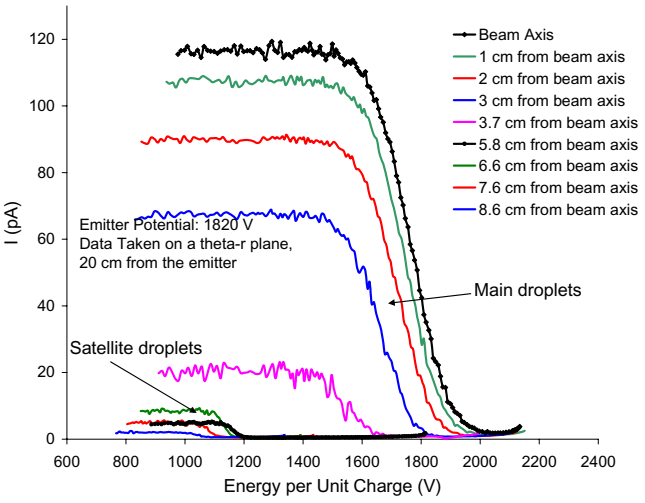

Figure 2. Retarding potential spectra of a 87 nA PC/EMI-Im electrospray, taken at different polar angles.

which is the statement of conservation of energy for a charged droplet. Taking "**x**" to be the position of the jet breakup point, "$\mathbf{x_B}$", and, if as an approximation, we assume that 1)the initial velocities of all droplets are the same and equal to the jet velocity, v_j, and 2)all droplets are generated at the same potential,

$$\phi_i^{RP} = \frac{1}{2}\frac{m_i}{q_i} v_j^2 + \phi(\mathbf{x_B}) \qquad [13]$$

v_j and $\phi(\mathbf{x_B})$ can be estimated with this expression, together with the experimental values of the retarding potential and specific charge of different droplets. With the data in figures 2, 3 and 4 we compute the following functions of the polar angle: the accumulated beam current, $I(\theta)$ (see figure 5), the average retarding potential of the droplets, $\tilde{\phi}(\theta)$, and the average (inverse) specific charge function, $\frac{\tilde{m}}{q}(\theta)$. When $\tilde{\phi}(\theta)$ is plotted versus $\frac{\tilde{m}}{q}(\theta)$, and a straight line fitted to the data, $\frac{1}{2}v_j^2$ can be computed from the slope of the fitting and $\phi(\mathbf{x_B})$ from its interception with the y-axes. This is shown in figure 6. From the straight line fitting, the velocity of the droplets at the jet breakup point is estimated to be 144 m/sec, while the electrical potential at this point would be 826 V. Additionally, from the value for the propellant flow rate and the jet velocity we can estimate the radius of the jet, $R_j = 96$ mm.

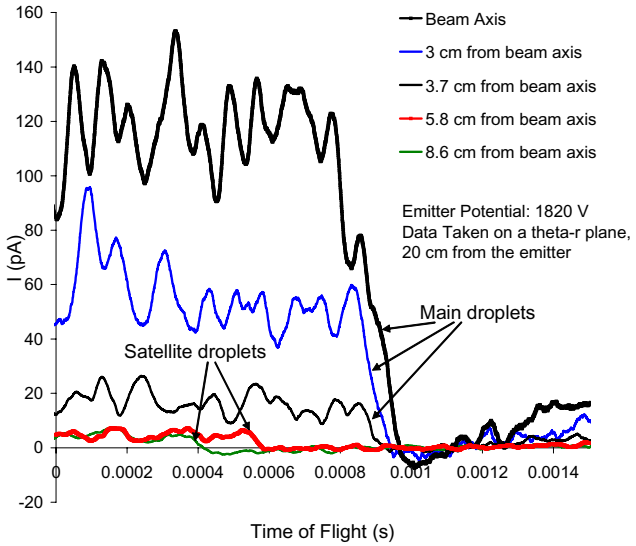

Figure 3. Time of flight spectra of a 87 nA PC/EMI-Im electrospray, taken at different polar angles.

C. Beam spreading solution and experimental validation

The spreading of the beam is computed with equations [1] to [8] and the estimates for the boundary conditions obtained in the previous section. First, we define the m groups in equation [1] using the accumulated beam current versus polar angle function shown in figure 5. For this calculation we divided the beam current into 9 groups of equal magnitude, centered at the following polar angles (deg): {2.63, 4.67, 6.17, 7.51, 8.79, 10.3, 16.7, 19.0}. The average specific charge for each polar angle θ_i, or group, is computed from the experimental data. The calculation is refined by further dividing each group 11 times.

The numerical solution of the system with 2x9x11 nonlinear coupled ODEs is shown in figure 7. The external electric field is computed with Maxwell 2D, and imputed to the particle trajectory integrating routine. The beamlets for particles of a given group have the same color. Note that there is some mixing of the beamlets associated with main droplets and different groups. On the other hand, the trajectories of the satellite droplets are separated from those of the main droplets, just as the experimental data in figures 2 to 4 show. This separation is due to the larger effect of the repulsive space charge forces on droplets with increased specific charge, and lower initial inertia (i.e. the satellite droplets).

Figure 8 shows the local angle of the trajectories. The local angles increase until maxima are reached and diminish afterwards. The position of the maxima coincide with the region where space charge transition from being the dominant force driving the droplet trajectories, to being negligible as compared to inertia and the external electric field force.

The comparison between the calculated and experimental beam spreading is shown in figure 9, in the form of accumulated beam current versus polar angle. For the calculated trajectories, the polar angle is defined as the local angle of the trajectories at the extractor electrode, since downstream of this point the external electric field is zero, the space charge forces remain negligible, and therefore the droplet trajectories become straight lines. Despite the simplifications of the model, such as the constant initial velocities and potential of the particles, and the neglect of the axial component of the space charge field, the model does a good job of predicting the spreading of the beam.

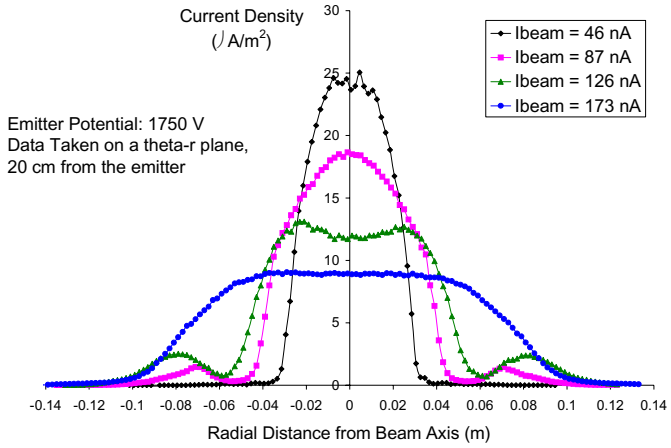

Figure 4. Beam profiles for different beam currents.

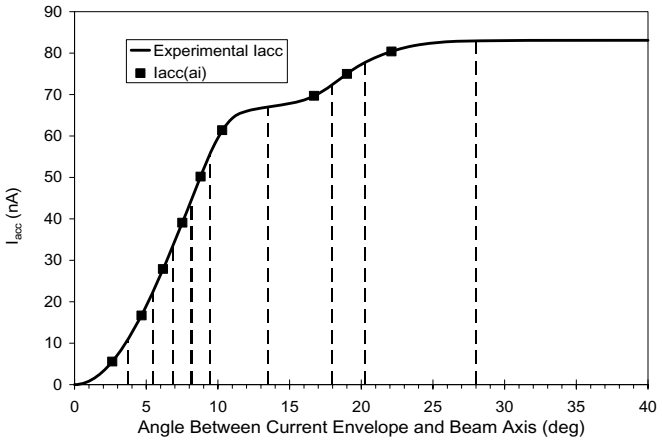

Figure 5. Accumulated beam current versus polar angle for I_B = 87 nA.

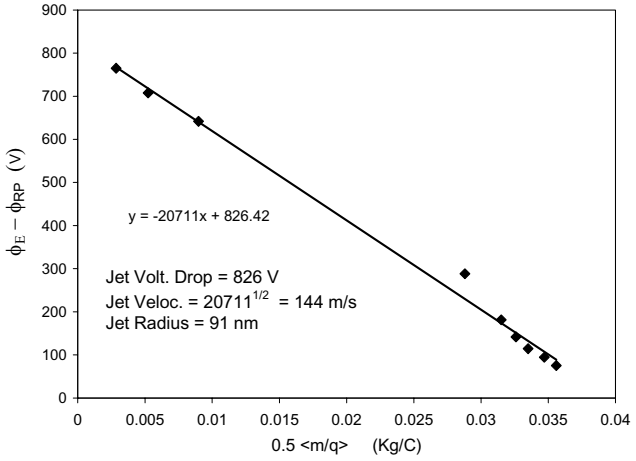

Figure 6. Estimation of droplet initial velocity and potential. Note that the y-axes displays the emitter voltage (1820 V) minus the droplet retarding potential.

III. Conclusion

We have presented a model for the spreading of colloid thruster beams in a vacuum. The model has been complemented with an experimental technique for estimating the velocity, potential and radial position of the beam droplets at their emission point, which are the initial conditions required to solve the model equations. The model is satisfactorily accurate, in the sense that reproduces the observed spreading of the colloid thruster beam. Currently we are using this tool to optimize the geometry of the electrospray source electrodes in order to increase the beam current (and hence the thrust) that can be extracted from the thruster, and reduce the divergence of the beam (which will minimize the potential for spacecraft contamination).

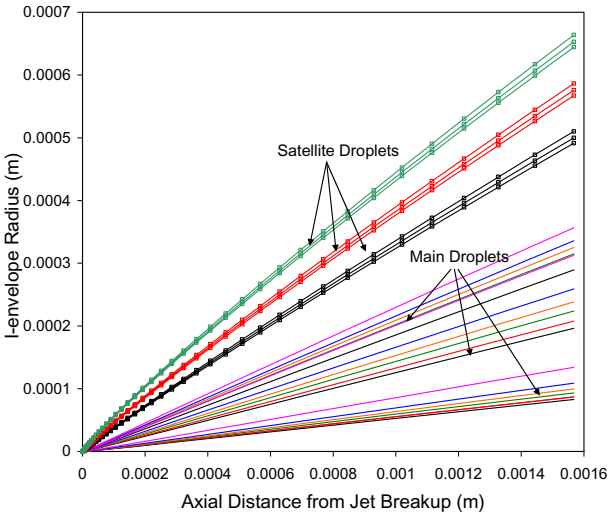

Figure 7. Beamlet envelope trajectories.

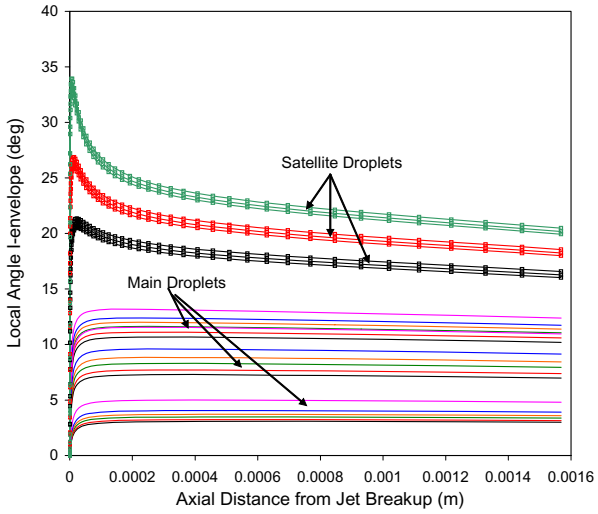

Figure 8. . Beamlet envelope local angles.

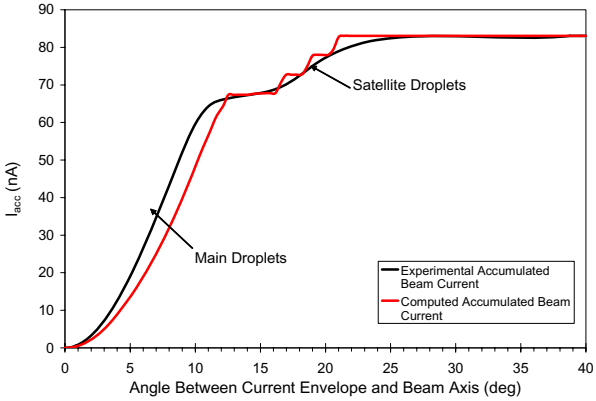

Figure 9. Computed and measured accumulated current versus polar angle .

Acknowledgments

The research described in this paper was carried out at the Jet Propulsion Laboratory, California Institute of Technology, under a contract with the National Aeronautics and Space Administration.

References

[1] M. Morse & H. Feshbach, "Methods of theoretical physics", pg. 1284, vol. II. New York, McGraw-Hill, 1953.

[2] M. Gamero-Castaño & V. Hruby, "Electric measurements of charged sprays emitted by cone-jets", Journal of Fluid Mechanics, 459, 245-276 (2002)